Magnetostrictive Néel ordering of the spin-5/2 ladder compound BaMn$_2$O$_3$: distortion-induced lifting of geometrical frustration

M. Valldor[1], O. Heyer[1], A. C. Komarek[1], A. Senyshyn[2], M. Braden[1], and T. Lorenz[1]

[1]*II. Physikalisches Institut, Universität zu Köln, Zülpicher Str. 77, 50937 Köln, Germany*
[2]*Technische Universität Darmstadt, Material und Geowissenschaften,*
Petersenstr. 23, 64287 Darmstadt, Germany and Technische Universität München,
FRM-II, Lichtenbergstr. 1, 85747 Garching, Germany
(Dated: October 8, 2010)

The crystal structure and the magnetism of BaMn$_2$O$_3$ have been studied by thermodynamic and by diffraction techniques using large single crystals and powders. BaMn$_2$O$_3$ is a realization of a $S = 5/2$ spin ladder as the magnetic interaction is dominant along 180° Mn-O-Mn bonds forming the legs and the rungs of a ladder. The temperature dependence of the magnetic susceptibility exhibits well-defined maxima for all directions proving the low-dimensional magnetic character in BaMn$_2$O$_3$. The susceptibility and powder neutron diffraction data, however, show that BaMn$_2$O$_3$ exhibits a transition to antiferromagnetic order at 184 K, in spite of a full frustration of the nearest-neighbor inter-ladder coupling in the orthorhombic high-temperature phase. This frustration is lifted by a remarkably strong monoclinic distortion which accompanies the magnetic transition.

I. INTRODUCTION

Exotic magnetic ground states are expected and have been observed in a special group of layered metal oxides containing spin ladders[1–6]. In the cuprates, these quasi-one dimensional magnetic units of $S = 1/2$ ($3d^9$) Cu^{2+} ions belong to the most well studied spin liquids and do not evolve long-range magnetic order at finite temperatures. This mainly arises from a very effective magnetic decoupling of neighboring spin ladders due to a geometrical frustration of the magnetic spin interactions present between the ladders. The strongest antiferromagnetic (AFM) spin-spin couplings J_1 and J_2 are expected, respectively, along the rungs and legs of the spin ladders due to almost perfect super-exchange conditions[7,8], which are responsible for interesting spin dynamics[9]. Small anisotropies in J within the ladders could also result in spin dimerization[10]. Furthermore, due to the low dimensionality of such spin-ladder materials they can act as model systems and connect theory with experiment in e.g. spectroscopy[11–14], thermal conductivity[15,16], and thermodynamics[17,18]. The spin-ladder structural features are still rare in nature, but are present in the metal oxide BaMn$_2$O$_3$[19]. The high spin moment $S = 5/2$ of Mn^{2+} ($3d^5$) represents a very different situation as for the cuprates, but theoretical work on the $S = 5/2$ model systems predicts dimerization[20]. Here, we present a combined study of magnetism, x-ray and neutron diffraction, and thermodynamic properties on BaMn$_2$O$_3$.

The room-temperature crystal structure of BaMn$_2$O$_3$ has been described by Sander and Müller-Buschbaum[19] and is shown in Fig. 1 (a). Similar to the hexagonal RMnO$_3$ (R = Ho–Lu, Sc, and Y)[21], Mn has a five-fold coordination, which forms an almost perfect trigonal bipyramid. However, the relatively lower oxygen content in BaMn$_2$O$_3$, i.e. the lower oxidation state of Mn, forces the MnO$_5$ polyhedra to also share edges instead of only corners. This condensation is known as "shear-planes" in
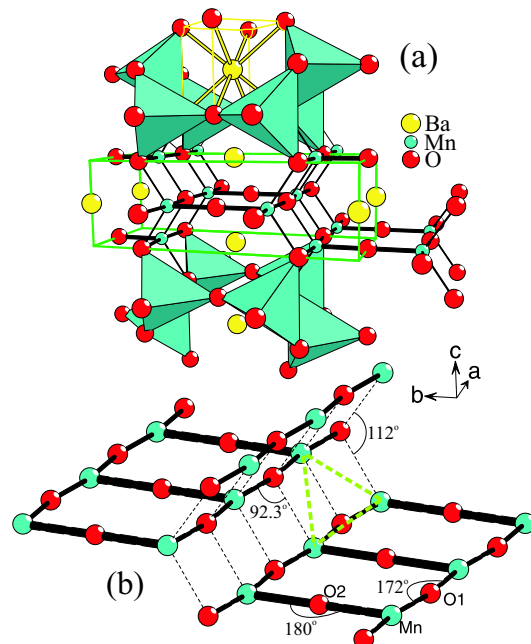

FIG. 1. (Color online) (a) Room temperature structure of BaMn$_2$O$_3$. The red balls at the corners of the Mn-containing polyhedra are oxygen atoms. The unit cell is indicated in green. The eightfold Ba coordination is indicated by yellow lines. (b) A selected part of the structure showing the Mn-O substructure with Mn–O–Mn bond angles. The dashed green lines indicate the geometrical frustration, as discussed in the text.

tungstenates[22] and causes the structure to evolve double layers of edge-sharing MnO$_5$ polyhedra, perpendicular to the b axis, with corner sharing as the only connection between these double layers. The Ba^{2+} ions fill the space between the layers and coordinate eight oxygen ions. The Mn–O–Mn super-exchange, however, is not governed by the double layers but by the bond angles and by the bond directions, shown in Fig. 1 (b), which amount to 180°

[010], 172° [100], 112° [001], and 92.3°, which should ensure strong magnetic coupling along the rungs (J_1) and the legs (J_2) of each ladder, but weaker interactions between them. The Mn–to–Mn interactions from one ladder to the nearest-neighboring ones constitute a complete geometric frustration. By symmetry the interactions are equally strong to the two next-nearest Mn^{2+} ions in the nearest-neighboring ladder (thick dashed lines in Fig. 1b). This results in a geometric frustration and in an effective decoupling of the neighboring ladders, and quasi 1D AFM interactions along the [100] axis are expected to dominate the magnetic correlations of $BaMn_2O_3$.

II. EXPERIMENTAL

A single crystal of centimeter size was synthesized using a floating-zone image furnace (FZ-T-10000-H-VI-VP) in a flowing gas mixture of $N_2/H_2(5\%)$ (0.25 dm^3/min). Both feeding bar and seed were pressed from stoichiometric amounts of $BaCO_3$ (Strem Chem. 99.9%) and MnO (Aldrich 99+%). The issue of BaO loss due to a transport reaction with H_2, as was mentioned in the first paper on this compound[19], could to some extent be avoided by growing the crystal at a relatively high rate of 10 mm/h. Indeed, the obtained crystal was covered by a thin layer of lime green crystals (MnO), indicating a small loss of BaO, but this top layer could be removed mechanically. Such a pure $BaMn_2O_3$ crystal appears dark, almost black, but thinner parts reveal that the compound is transparent and dark forest-green. The pale yellow color observed in Ref. 19 can be seen if the crystals are further crushed, reaching micrometer size. The compound decomposes slowly in air, but relatively fast in water. Both reactions cause the crystal surface to become brown, probably due to formation of Ramsdellite (α-MnO_2) and barium hydroxides and carbonates.

Elemental analysis was performed in a scanning electron microscope SEM515 (Philips) equipped with an EDX unit at 20 kV acceleration voltage. The average metal-to-metal composition was determined to be $Ba_{1.002(8)}Mn_{1.998(8)}$ from 10 EDX analyses at different spots on a centimeter-sized single-crystal slice; this very well agrees with the expected metal stoichiometry. The purity of the sample was checked by powder X-ray diffraction and no impurity phases could be detected meaning that the sample is at least 95% pure.

The X-ray powder diffraction data were collected at 300 K using a Cr $K_{\alpha_{1,2}+\beta}$ X-ray tube (λ = 2.28973, 2.29365, and 2.08090 Å) as source. The intensities were collected in reflection (Bragg-Brentano) geometry. Single crystal X-ray measurements were performed down to 100 K with a Bruker X8 APEX (Mo$K_{\alpha_{1,2}}$, λ = 0.7093 and 0.71359 Å); the cooling was accomplished by using a flow of dry N_2 gas (Cryoflex). Neutron diffraction data was collected at SPODI, FRM II (Munich, Germany), with a constant wavelength of 2.537 Å(Ge [331] monochromator) at temperatures between 3 and 300 K.

A vanadium cup was used as sample holder for the powdered single crystal sample.

Magnetic and specific-heat measurements were performed in a commercial Physical-Properties-Measurement-System (PPMS, Quantum Design Inc.) in the temperature range 2-400 K in magnetic fields up to 14 T. The magnetization was measured by the vibrating-sample technique while either the magnetic field or the temperature is continuously varied. For the specific heat, a relaxation-time method is used and the data points are typically obtained step-wise after stabilizing certain temperatures. In addition, we also used a quasi-continuous modification of this relaxation-time method (see Ref. 23) in the temperature range around the first-order phase transition. Thermal expansion was investigated on a home-built high-resolution capacitance dilatometer.

To ensure that the sample did not deteriorate in air, the crystal was only handled in an Ar-filled glove box and sealed in a shrink hose before performing the magnetic measurements. For all the other methods the crystals were rapidly transferred in air from the Ar-filled glove box to the respective measurement setups, which work either in He atmosphere, dry N_2 gas or under vacuum conditions. In none of the measurements on $BaMn_2O_3$ single crystals we could observe indications for the presence of a sizeable amount of impurity phases. This was different for the neutron powder diffraction data which revealed that the studied sample contains about 3 % of MnO. This impurity phase in the neutron data probably originates from the fact that the exposure to air is more severe for a powdered sample with a much larger surface-to-volume ratio than a single crystal.

III. THERMODYNAMIC PROPERTIES

Fig. 2 summarizes the magnetic measurements. Between about 200 and 400 K, the magnetic susceptibility χ shows a weak anisotropy with respect to the direction of the applied magnetic field. The data of Fig. 2 have been obtained after cooling the sample in zero magnetic field. The corresponding data from field-cooling experiments (not shown) perfectly superimpose these data for all three field directions, which rules out the existence of some type of ferromagnetic domains or a spin-glass behavior in $BaMn_2O_3$. For all three field directions, the temperature dependencies $\chi_i(T)$ strongly deviate from a simple Curie-Weiss behavior. Instead the $\chi_i(T)$ show broad maxima which, depending on the field direction i, are located between about 250 and 290 K. These broad maxima are typical for low-dimensional magnets and signal the continuous increase of magnetic correlations with decreasing temperature. The susceptibility data unambiguously proves the low-dimensional nature of magnetic correlations in $BaMn_2O_3$. At $\simeq$ 184 K clear anomalies occur in all three $\chi_i(T)$: for a field along the orthorhombic a axis, χ_a strongly decreases and levels off at a very
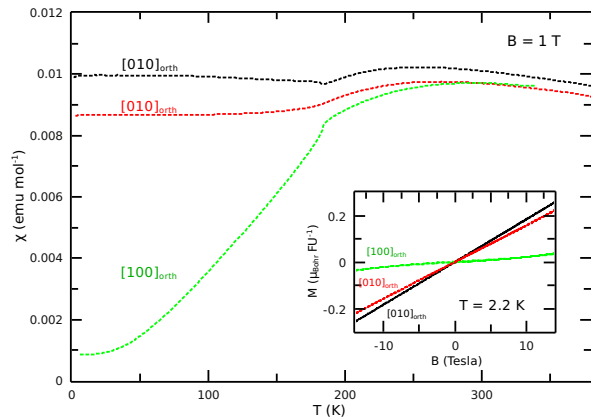
FIG. 2. (Color online) Magnetic susceptibility as a function of temperature measured in magnetic fields of 1 T applied along all three orthorhombic crystallographic directions of BaMn$_2$O$_3$. The inset displays magnetization curves measured at 2.2 K as a function of the magnetic field up to 14 T applied along the orthorhombic axes.

small value at the lowest temperature, while for a field along the orthorhombic b (c) axis χ_i slightly increases (decreases) below 184 K and finally remains essentially constant below about 100 K. This anisotropic behavior is a clear indication of an antiferromagnetic ordering, where, below the Néel temperature $T_N \simeq 184$ K, the spins spontaneously align predominantly (anti)parallel to the orthorhombic a axis.

The low-temperature magnetization measured as functions of magnetic fields up to 14 T applied along these three field directions are shown in the inset of Fig. 2. Obviously, there are neither indications of metamagnetic transitions nor of a magnetic hysteresis. Instead, these data show that the low-field anisotropy observed in the temperature-dependent measurements at 1 T remains essentially preserved up to a field of 14 T. At first glance, this is a surprising observation, because for the $3d^5$ configuration of Mn^{2+} the orbital contribution to the magnetic moment is typically small and consequently the magnetic anisotropy is expected to be weak. In other words, Mn^{2+} systems are expected to represent rather well the spin-5/2-Heisenberg system. In this case, however, only a weak magnetic anisotropy is expected and comparatively low magnetic fields along the easy a axis should be sufficient to induce a so-called spin-flop transition, where the spin orientation changes from being (anti)parallel to the a axis to a direction within the plane perpendicular to a.

A rough estimate of the effective intra-ladder couplings can be obtained by comparing the positions of the susceptibility maxima of BaMn$_2$O$_3$ to Monte Carlo simulations of $S = 5/2$ ladders[20]. According to these simulations the susceptibility maximum is expected to occur at $T \simeq 6.69J$ for a homogeneous spin ladder with equal rung and leg coupling $J_1 = J_2 = J$. Thus, our data suggest an intra-ladder coupling $J \simeq 40$ K. Due to the
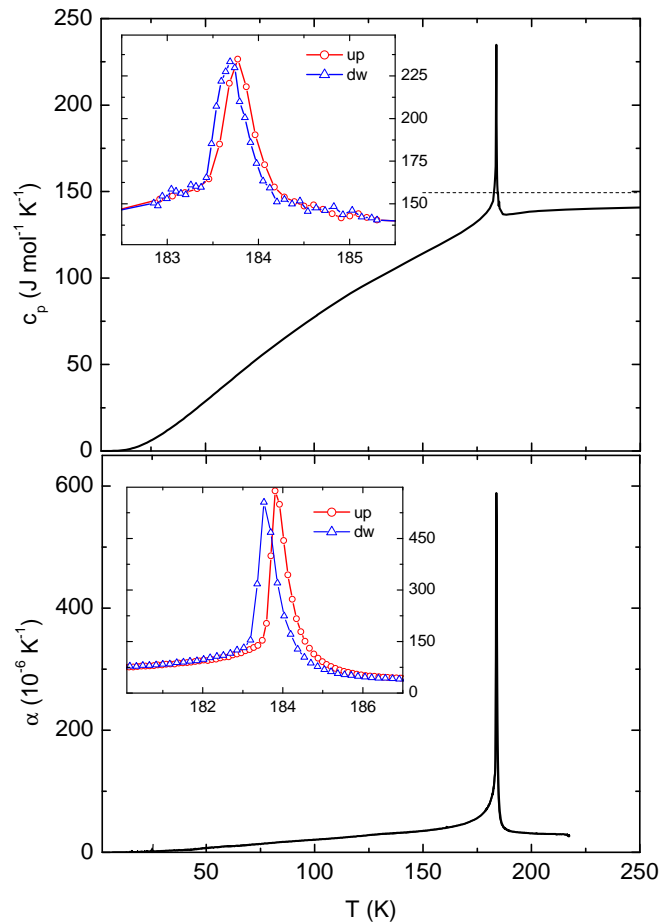

FIG. 3. (Color online) Specific heat (top) and linear thermal expansion (bottom) of BaMn$_2$O$_3$ in zero magnetic field. Thermal expansion was measured along $[001]_{orth}$ direction. The dashed line in the upper panel marks the Dulong-Petit limit. In both panels, the inset is a blow-up of the respective heating (up) and cooling (dw) curves in the temperature range close to the Néel ordering.

large spin value, this coupling corresponds to a very large saturation field $H_{sat} = 2Sk_B(2J_1 + J_2)/g\mu_B \simeq 450$ T. In view of this large saturation field, the absence of a spin-flop transition in the studied field range appears less surprising, because from the present data one can only conclude that the spin-flop field H_{SF} is larger than 14 T, i.e. $H_{SF}/H_{sat} > 3$ %. Within a mean-field treatment[24], this can be explained already by a very weak anisotropy field $H_A/H_{sat} > 10^{-3}$. A closer inspection of the data in the inset of Fig. 2 reveals a weak increase of slope in the high-field region of the magnetization curve for a field applied along a. Thus, one may speculate that a spin-flop transition could occur in the field range slightly above our maximum field. In order to clarify this issue, measurements to higher fields are necessary.

In the specific heat, shown in Fig. 3a, a pronounced anomaly appears close to 184 K, which signals a release in entropy. The specific-heat peak is slightly asymmetric, λ-like, which would infer that the phase transition is

TABLE I. Single crystal X-ray data of $BaMn_2O_3$ at 150 and 100 K. Each atomic site is presented as follows: Atom, occ., x, y, z, U_{iso}, U_{11}, U_{22}, U_{33}, U_{12}, U_{13}, U_{23} with STDs in parentheses. (*adopted from the neutron powder diffraction data at the same temperature).

Temperature (K)	150	100
$2a$	Ba, 1.0, 0, 0, 0, 0.0069(1), 0.0074(1), 0.0069(1), 0.0071(1), 0, 0.004988(8), 0	Ba,1.0, 0, 0, 0, 0.00512(9), 0.00569(9), 0.00515(9), 0.00532(9), 0 0.00384(7), 0
$4g$	Mn, 1.0, 0, 0.31183(3), 0, 0.0068(2), 0.0068(2), 0, 0.31183(3), 0, 0.00432(8), 0.0056(1),	Mn, 1.0, 0, 0.31183(3), 0, 0.00432(8), 0.0056(1), 0.0050(1), 0.0059(1), 0, 0.0037(1), 0
$2b$	O, 1.0, 0, 1/2, 0, 0.0092(9), 0.0098(9), 0.0061(7), 0.0112(9), 0, 0.0065(8), 0	O, 1.0, 0, 1/2, 0, 0.0075(9), 0.0093(9), 0.0043(7), 0.0094(8), 0, 0.0061(7), 0
$4h$	O, 1.0, 0, 0.2036(2), 1/2, 0.0085(6), 0.0076(6), 0.0089(6), 0.0090(6), 0, 0.0053(5), 0	O, 1.0, 0, 0.2036(1), 1/2, 0.0069(6), 0.0063(5), 0.0071(5), 0.0074(5), 0, 0.0043(5), 0
Space group (Nr.)	$C2/m$ (12)	$C2/m$ (12)
a, b, c (Å)*	5.62060(2), 10.96155(3), 3.53794(2)	5.61194(2), 10.95766(3), 3.53324(2)
α, β, γ (°)*	90, 128.8199(2), 90	90, 128.7261(1), 90
S (obs, all)	1.21, 1.21	1.16, 1.17
R(obs, all)	0.0189, 0.0189	0.0175, 0.0175
R_w(obs, all)	0.0546, 0.0547	0.0518, 0.0518
Refined str. factor	F^2	F^2
Z	2	2
Transm. min/max.	0.0659/0.1291	0.0980/0.1714
Abs. coeff	18.527 mm^{-1}	18.555 mm^{-1}
F(000)	260	260
Ref. total	561	563
Ref.($I > 3\sigma$)	557	561
Peak/hole	0.87/-1.24 e/Å^3	0.95/-1.25 e/Å^3

of second order. However, measurements with increasing and decreasing temperature reveal a small hysteresis of $\simeq 0.2$ K (inset of Fig. 3a), which identifies this transition as a weak first-order one. In Fig. 3b, we show the linear thermal expansion measured along the [001] direction according to the orthorhombic settings. Again, a strong anomaly is observed close to 184 K, with a minor thermal hysteresis of about 0.2 K between the curves measured on increasing and decreasing temperature, in very good agreement with the results of the specific heat data. The magnitude of the thermal-expansion anomaly at T_N is huge, which reveals that this magnetic ordering strongly couples to the lattice. The strong magnetoelastic coupling is also the most likely reason for the first-order nature of this phase transition. It has been shown that an intrinsically second-order phase transition can be driven to first order by a finite coupling to the lattice[25,26].

From the presented macroscopic data the behavior of $BaMn_2O_3$ may be summarized as follows: $BaMn_2O_3$ contains 2-leg spin ladders with spin 5/2 and a rather strong intra-ladder coupling of the order of $J \simeq 40$ K as inferred from the broad susceptibility maxima around 270 K. Despite this large coupling, a three-dimensional Néel order is suppressed because the effective inter-ladder coupling is weak as a consequence of the geometrical arrangement

of neighboring ladders that causes strong magnetic frustration. Nevertheless, $BaMn_2O_3$ undergoes an antiferromagnetic ordering transition at T=184 K. In order to allow for a three-dimensional Néel ordering, this frustration can be lifted by a structural distortion, which then naturally explains the strong magnetoelastic coupling and the weakly first-order nature of the observed phase transition at 184 K. In order to resolve the microscopic details of these structural changes and the magnetic structure we performed single-crystal X-ray measurements down to 100 K as well as neutron powder diffraction measurements on a crushed single crystal in the temperature range from 3 to 300 K.

IV. CRYSTALLOGRAPHIC AND MAGNETIC STRUCTURE

Fig. 4 displays the X-ray powder diffraction data obtained from a crushed piece of the $BaMn_2O_3$ single crystal. The structure refinement with these data using Fullprof2k[27] yields the unit-cell parameters $a = 4.3819(1)$ Å, $b = 10.9745(5)$ Å, and $c = 3.55329(8)$ Å, in good agreement with $a = 4.385$ Å, $b = 10.967$ Å, and $c = 3.552$ Å reported previously[19]. Our room-
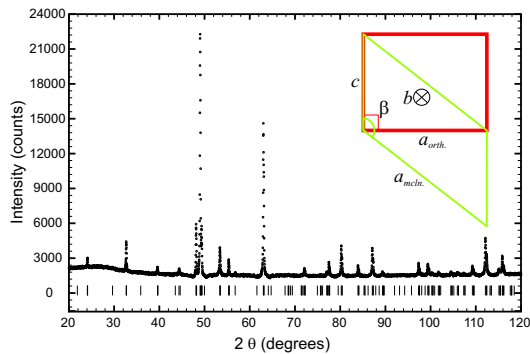
FIG. 4. (Color online) Room temperature X-ray powder diffraction pattern of $BaMn_2O_3$. The observed intensities are marked by open circles and the expected Bragg positions by vertical lines. The upper-right inset displays the orthorhombic and the monoclinic unit cells in the ac plane.

temperature X-ray diffraction data perfectly agree with the already reported $Immm$ symmetry. However, the low-temperature data (at 150 and 100 K) of a $BaMn_2O_3$ single crystal, see Table I, clearly indicate a lower monoclinic symmetry $C2/m$ (see inset in Fig. 4), as choices with higher symmetries cannot index all observed intensities.

In Fig. 5, two representative neutron powder diffraction patterns are shown and the results of Rietveld refinements for five different temperatures are summarized in Table II. The data of Fig. 5 reveal that the sample contains about 3 % of MnO as an impurity phase. This impurity phase in the neutron data probably originates from the fact that the powdered sample was exposed to air before placing it in the vanadium cup. A partial decomposition of the sample explains this minor complication in the neutron data, but there is no evidence of an antiferromagnetic ordering transition at 118 K in the magnetic investigations, which would be expected if a significant amount of MnO was present in the original single crystal as well.

According to the thermodynamic data (see above), $BaMn_2O_3$ orders magnetically at 184 K and, indeed, magnetic Bragg peaks are visible at 180 K. Simultaneously, several nuclear peaks split indicating that the symmetry is lowered, in agreement with the lowering to the monoclinic symmetry obtained from the low-temperature single crystal X-ray data. An example of the splitting is shown in Fig. 6a; the two intensities, indexed as [152] ($2\Theta = 149.5°$) and [321] ($2\Theta = 150.6°$) in the centered orthorhombic setting ($Immm$), shift only slightly between 200 and 190 K, due to shrinkage of the unit cell, but at 170 K both peaks are clearly split and their intensities are distributed. Due to the high scattering angle we may safely neglect any magnetic scattering as possible cause of the peak splitting.

The emergence of the magnetic Bragg peaks upon cooling is shown for the example of the (1 1 -1/2)/(1 -1 -1/2) reflection in Fig. 6b). This purely magnetic intensity de-
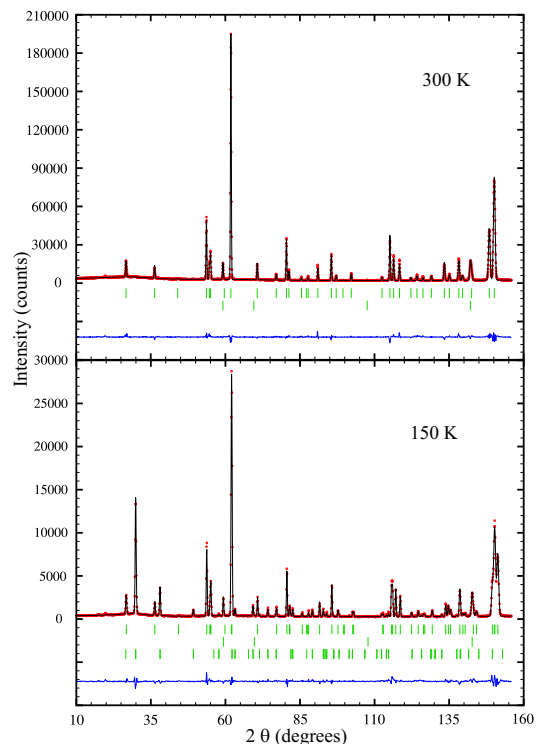

FIG. 5. (Color online) Neutron diffraction data of $BaMn_2O_3$ at 300 (top) and 150 K (bottom). Observed intensities are marked by circles and the calculated pattern as a line. All Bragg intensities are indicated by vertical lines: $BaMn_2O_3$ (1st row), MnO (2nd row), and $BaMn_2O_3$ spin structure (3rd row). The lowest line is the difference between observed and calculated intensities $I_{obs} - I_{calc}$.

velops from a diffuse scattering, which is present already at 200 K as a broad hump on top of the background intensity. At 190 K, the diffuse scattering sharpens, which means that the spin-spin correlation length increases, and at 180 K, this peak exhibits a well-defined half width, close to that of the nuclear scattering intensities at similar scattering angle, e.g. $[020]_{mcln}$.

To enable unit cell comparisons between all temperatures, the monoclinic unit cell was refined on all diffraction data and the result is shown in Fig. 7. The lattice constants a, b, and c decrease continuously on cooling between 300 and 50 K, but a changes much stronger than b and c. A small anomaly in the a parameter is visible on cooling through T_N. As shown in the inset of Fig. 7, the monoclinic angle β indicates that the structure distorts below 180 K. Above 200 K, the value of β was fixed to the value calculated via the orthorhombic lattice constants, see inset of Fig. 4. In the bottom panel of Fig. 7 we show the ordered Mn^{2+} magnetic moment as a function of temperature.

All magnetic Bragg peaks appearing below $T_N \simeq$ 184 K can be indexed with the propagation vector k=(0 0 1/2), i.e. by a doubling of the c axis. This means that the next-nearest neighbor ladders connected by one c-lattice spacing are ordering antiferromagnetically, whereas the

TABLE II. Atomic and magnetic parameters of $BaMn_2O_3$ at different temperatures. All atomic positions are assumed to be fully occupied and STDs are already multiplied by the Berar-Lelann factor[28] and an additional factor of three to compensate for pronounced texture effects in the raw data[29]. Data for MnO was taken from G.R. Levi[30] and Goodwin *et al.*[31].

Temperature (K)	300	200	150	100	3
Ba (x, y, z, U_{iso})	1/2, 1/2, 0, 0.0073(5)	1/2, 1/2, 0, 0.0045(4)	0, 0, 0, 0.0054(7)	0, 0, 0, 0.0073(6)	0, 0, 0, 0.0033(9)
Mn (x, y, z, U_{iso})	1/2, 0.1882(1), 0, 0.0130(5)	1/2, 0.18811(9), 0, 0.0132(4)	0, 0.3125(9), 0, 0.0085(7)	0, 0.3124(9), 0, 0.0094(7)	0, 0.312(1), 0, 0.0075(9)
O1 (x, y, z, U_{iso})	0, 1/2, 1/2, 0.0190(5)	0, 1/2, 1/2, 0.0172(4)	0, 1/2, 0, 0.0116(7)	0, 1/2, 0, 0.0127(7)	0, 1/2, 0, 0.0144(9)
O2 (x, y, z, U_{iso})	0, 0.2048(1), 0, 0.0176(4)	0, 0.20423(9), 0, 0.0161(3)	0, 0.2039(2), 1/2, 0.0157(5)	0, 0.20402(9), 1/2, 0.0154(5)	0, 0.2030(1), 1/2, 0.0101(6)
Space Group (Nr.)	*Immm* (71)	*Immm* (71)	*C2/m* (12)	*C2/m* (12)	*C2/m* (12)
a (Å)	4.3834(1)	4.38006(6)	5.62060(6)	5.61194(6)	5.60595(6)
b (Å)	10.9751(2)	10.96636(9)	10.96155(9)	10.9577(1)	10.9553(1)
c (Å)	3.5549(1)	3.54433(6)	3.53794(6)	3.53324(6)	3.53000(6)
β (°)	90	90	128.8199(3)	128.7261(3)	128.6678(3)
χ^2	4.23	2.23	7.92	4.35	5.38
R_{Bragg}	0.0572	0.0448	0.0482	0.0584	0.0704
R_F	0.0556	0.0412	0.0443	0.0433	0.0529
Magn. k vector	—	—	[0,0,1/2]	[0,0,1/2]	[0,0,1/2]
R_{mag}	—	—	0.117	0.0985	0.0955
Comment	MnO 3.13(6)%	MnO 3.09(6)%	MnO 2.94(6)%	MnO excluded	MnO excluded

next-nearest neighbor ladders connected by one *b*-lattice spacing are coupled ferromagnetically. The coupling along *c* is mediated by the J_3 parameter, which the magnetic symmetry determines to be antiferromagnetic. Due to the 180° Mn-O-Mn bonds there is no doubt that the intra-ladder interaction parameters J_1 and J_2 must be antiferromagnetic, which unambiguously fixes the magnetic order within a single ladder. With these arguments we determine the magnetic structure including the inter-ladder coupling between ladders connected by one *c* or by one *a* lattice parameter. What has not been discussed so far is the coupling between nearest-neighbor ladders connected by the body centering of the orthorhombic lattice $(1/2,1/2,1/2)$. However, the two choices of ferromagnetic and antiferromagnetic coupling do not result in different symmetries but only in two different domain types. Choosing a ferromagnetic coupling for $(1/2,1/2,1/2)$ yields an antiferromagnetic coupling for $(1/2,-1/2,1/2)$ and *vice versa*. The magnetic symmetry constructed above is monoclinic and the two domain types correspond to the common symmetry reduction from orthorhombic to monoclinic. As already discussed above, the Mn moment is dominantly oriented along the *a* axis and a picture of the spin structure in comparison with the ladders is shown in Fig. 8. With this magnetic model the neutron powder-diffraction data is perfectly described. The Mn^{2+} ordered moment rapidly increases and half of the expected 5 μ_B is observed already at 170 K. With further decreasing temperature, the moment further increases and finally saturates at $\simeq 4.7$ μ_B close to the expected value.

The role of the monoclinic structural distortion in $BaMn_2O_3$ has to be discussed concerning two aspects. First, the monoclinic distortion is just a consequence of the monoclinic magnetic symmetry; but thereby one would only expect a weak structural deformation. Second, the monoclinic distortion lifts the magnetic frustration and thereby stabilizes the magnetic order in $BaMn_2O_3$ significantly. The nearest-neighbor inter-ladder interaction parameters J_4 and J_4' are mediated via Mn–O–Mn bonds close to a 90° configuration. In the high-temperature phase, both Mn–O–Mn angles are 92.3° (Fig. 1b), which causes a perfect geometrical frustration. On cooling through T_N, the structure changes from orthorhombic to monoclinic and induces an antisymmetric shift of the ladders, which changes the corresponding Mn–O–Mn angles by ±0.3° and lifts the perfect geometrical frustration. According to the Goodenough-Kanamori rules[7,8], a decreasing Mn–O–Mn angle results in a monotonic decrease from a large antiferromagnetic coupling at an 180° bond to a weak ferromagnetic coupling at a 90° bond. Thus one might expect J_4' with the larger angle of 92.61° to be increased while J_4 with the smaller angle of 92.01° to be decreased. This is, however, in contrast to our neutron data, which clearly show that the neighboring spins coupled via the larger bond angle of 92.61° are aligned parallel; see Fig. 8. This means that J_4 is larger than J_4' what most probably means that the minimum in the Mn–O–Mn angular dependence is located at a bond angle above 93°.

Due to the strong sensitivity of the magnetic interaction on this bond angle a sizeable magnetoelastic ef-
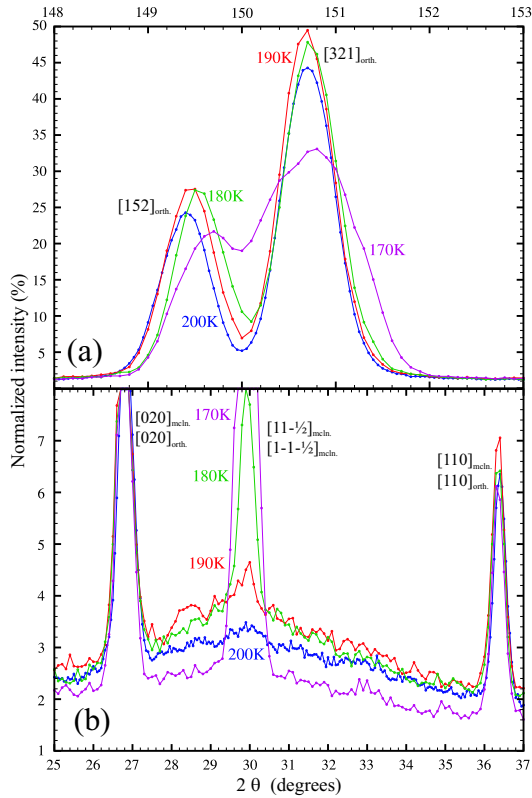
FIG. 6. (Color online) Representative neutron diffraction data at four temperatures. (a) Two of the peaks from the high-temperature orthorhombic structure are indexed and the splitting of, especially the [321] peak, is made clear. (b) The growth of the largest magnetic peak displayed at the same temperatures as in (a) and indexed according to high- and low-temperature crystallographic settings.

fect occurs in $BaMn_2O_3$, similar to the spin-Peierls compound $CuGeO_3$ where dimerization mainly arises from a Cu-O-Cu bond-angle modulation[33,34]. A similar lifting of geometric frustration through a coupled structural and magnetic transition has been reported recently for $VOCl$[35] and seems to be relevant in the parent phase of the iron-arsenide superconductors as well. In LaOFeAs the magnetic order is associated with a tetragonal-to-orthorhombic transition which also has a two-fold role[36]. It is a consequence of the lower magnetic symmetry and it lifts a magnetic frustration thereby stabilizing the magnetic order in full analogy to the discussion presented above for $BaMn_2O_3$.

V. CONCLUSIONS

We have presented a detailed study of large single crystals of $BaMn_2O_3$ grown in a floating-zone image furnace. $BaMn_2O_3$ has structural motifs from both the hexagonal $RMnO_3$[21] and the well-known spin-ladder compound $(Sr,Ca)_{14}Cu_{24}O_{41}$[32]. Although $BaMn_2O_3$ contains spin ladders with obvious geometrical frustration,
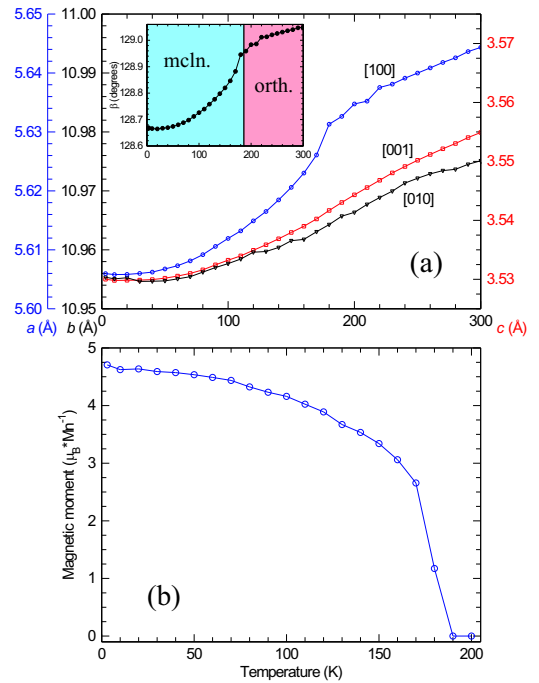

FIG. 7. (Color online) (a) The monoclinic unit-cell parameters, the β angle (inset), and (b) the ordered magnetic moment of Mn^{2+} as functions of temperature.
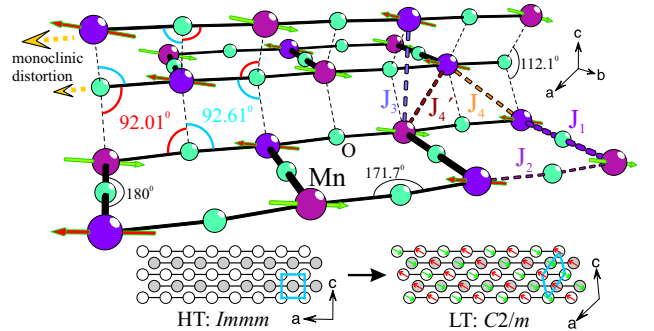

FIG. 8. (Color online) The magnetic structure of $BaMn_2O_3$ at 3 K, represented on its Mn-O sublattice. The magnetic moments of Mn are represented by arrows. The thick dashed lines represent the different Mn–to–Mn couplings (J_1–J_4). The arrows on the left show the ladder shift through the monoclinic distortion, as discussed in the text. The bottom panels compare the high-temperature (HT) and low-temperature structures of $BaMn_2O_3$.

this compound shows long-range antiferromagnetic order at $T_N \simeq 184$ K. The magnetic ordering is accompanied by a distortion of the crystal structure, which is described by a lowering of the symmetry from orthorhombic to monoclinic. Data from both specific-heat and thermal-expansion measurements clearly indicate that this phase transition shows a weak temperature hysteresis. The weak first-order feature of this magnetically driven phase transition is attributed to a strong magnetoelastic cou-

pling. The magnetic correlations above T_N are most likely confined within the ladders, which cannot show long-range order due to the low dimensionality of the (almost) isotropic Heisenberg spin system. The low dimensionality of the magnetic subsystem of $BaMn_2O_3$ is a consequence of a very effective magnetic decoupling between neighboring spin ladders due a perfect geometrical frustration. Experimentally, this low dimensionality is reflected by broad maxima in the temperature dependence of the magnetic suceptibility, which are located around 270 K suggesting an average intra-ladder coupling $J \simeq 40$ K. The low dimensionality is also clearly seen in the neutron diffraction data, where pronounced short-range magnetic correlations are observed already well above T_N. The neutron data reveal that at T_N the magnetic correlations become long-range and, in addition, there is an antisymmetric shift of neighboring spin lad-

ders, which results in an alternation of the corresponding Mn–O–Mn angles along the ladder direction. As a consequence, the geometrical frustration is lifted, the spin ladders become three-dimensionally coupled and, simultaneously, the magnetic subsystem develops long-range antiferromagnetic order. This indicates, that the structural phase transition from orthorhombic to monoclinic in $BaMn_2O_3$ is driven by a gain in the magnetic free energy.

[1] E. Dagotto, J. Riera, and D. Scalapino. Phys. Rev. B **45**, 5744 (1992).

[2] S.R. White, I. Affleck, and D.J. Scalapino. Phys. Rev. B **65**, 165122 (2002).

[3] S.T. Carr and A.M. Tsvelik. Phys. Rev. B **65**, 195121 (2002).

[4] T. Vuletic, B. Korin-Hamzic, T. Ivek, S. Tomic, B. Gorshunov, M. Dressel, and J. Akimitsu. **428**, 169 (2006).

[5] Z. Hiroi, M. Azuma, M. Takano, and Y. Bando. J. of Solid State Chem. **95**, 230 (1991).

[6] E. Dagotto and T.M. Rice. Science **271**, 618 (1996).

[7] J.B. Goodenough. Phys. Rev. **100**, 564 (1955).

[8] J. Kanamori. J. Phys. Chem. Solids **10**, 87 (1959).

[9] R.S. Eccleston, M. Azuma, and M. Takano. Phys. Rev. B **53**, 14721 (1996).

[10] M. Martin-Delgado, J. Dukelsky, and G. Sierra. Physics Lett. A **250**, 430 (1998).

[11] M. Windt, M. Grüninger, T. Nunner, C. Knetter, K.P. Schmidt, G.S. Uhrig, T. Kopp, A. Freimuth, U. Ammerahl, B. Büchner, and A. Revcolevschi, Phys. Rev. Lett. **87**, 127002 (2001).

[12] M. Klanjšek, H. Mayaffre, C. Berthier, M. Horvatić, B. Chiari, O. Piovesana, P. Bouillot, C. Kollath, E. Orignac, R. Citro, and T. Giamarchi, Phys. Rev. Lett. **101**, 137207 (2008).

[13] Ch. Rüegg, K. Kiefer, B. Thielemann, D. F. McMorrow, V. Zapf, B. Normand, M. B. Zvonarev, P. Bouillot, C. Kollath, T. Giamarchi, S. Capponi, D. Poilblanc, D. Biner, and K. Krämer, Phys. Rev. Lett. **101**, 247202 (2008) .

[14] B. Thielemann, Ch. Rüegg, H. M. Rønnow, A. M. Läuchli, J.-S. Caux, B. Normand, D. Biner, K.W. Krämer, H.-U. Güdel, J. Stahn, K. Habicht, K. Kiefer, M. Boehm, D. F. McMorrow, and J. Mesot, Phys. Rev. Lett. **102**, 107204 (2009).

[15] A. V. Sologubenko, K. Giannò, H. R. Ott, U. Ammerahl, and A. Revcolevschi, Phys. Rev. Lett. **84**, 2714 (2000).

[16] C. Hess, C. Baumann, U. Ammerahl, B. Büchner, F. Heidrich-Meisner, W. Brenig, and A. Revcolevschi, Phys. Rev. B **64**, 184305 (2001).

[17] T. Lorenz, O. Heyer, M. Garst, F. Anfuso, A. Rosch, C. Rüegg, and K. Krämer, Phys. Rev. Lett. **100**, 067208

(2008).

[18] F. Anfuso, M. Garst, A. Rosch, O. Heyer, T. Lorenz, C. Rüegg, and K. Krämer, Phys. Rev. B **77**, 235113 (2008).

[19] K. Sander and H. K. Müller-Buschbaum. Z. Anorg. Allg. Chem. **451**, 35 (1979).

[20] V. Tangoulis. Chem. Phys. **332**, 271 (2007).

[21] J.S. Zhou, J.B. Goodenough, J.M. Gallardo-Amores, E. Moran, M.A. Alario-Franco, and R. Caudillo. Phys. Rev. B **74**, 014422 (2006).

[22] L. Kihlborg and W. Israelss.m. Acta Chem. Scand. **22**, 1685 (1968).

[23] J.C. Lashley, M.F. Hundley, A. Migliori, J.L. Sarrao, P.G. Pagliuso, T.W. Darling, M. Jaime, J.C. Cooley, W.L. Hults, L. Morales, D.J. Thoma, J.L. Smith, J. Boerio-Goates, B.F. Woodfield, G.R. Stewart, R.A. Fisher, and N.E. Phillips. Cryogenics **43**, 369 (2003).

[24] L.J. Dejongh and A.R. Miedema. Adv. in Phys. **23**, 1 (1974).

[25] L.P. Kadanoff, W. Gotze, D. Hamblen, R. Hecht, E.A.S. Lewis, W. Palciaus.vv, M. Rayl, J. Swift, D. Aspnes, and J. Kane. Rev. Mod. Phys. **39**, 395 (1967).

[26] T. Ito, K. Ito, and M. Oka. Jpn. J. Appl. Phys. **17**, 371 (1978).

[27] T. Roisnel and J. Rodriguez-Carvajal. Fullprof2k V. 1.8a Laboratoire Leon Brillouin (CEA-CNRS) 91191 Gif-sur-Yvette Cedex (France) (2001).

[28] J.F. Berar and P. Lelann. J. Appl. Crystallogr. **24**, 1 (1991).

[29] The full two-dimensional analysis of the neutron powder data exhibited internal structure, because the powder contained comparatively large grains. To correct this effect in the Rietveld refinement we used an enhanced absorption correction and multiplied all standard deviations from the refinements by an additional factor of three. This factor was estimated by comparing the data from the refinement with the larger absorption with those from a refinement with a correct absorption correction which, however, yields negative thermal displacements.

[30] G. R. Levi. Rendiconti dell'Istituto Lombardo di Science e Lettere Classe di Science Mathematiche e Naturali **57**, 619 (1924).

[31] A.L. Goodwin, M.G. Tucker, M.T. Dove, and D.A. Keen. Phys. Rev. Lett. **96**, 047209 (2006).

[32] S.M. Kazakov, J. Karpinski, G.I. Meijer, C. Bougerol-Chaillout, and M. Nunez-Regueiro. Physica C **351**, 301 (2001).

[33] W. Geertsma and D. Khomskii. Phys. Rev. B **54**, 3011 (1996).

[34] M. Braden, G. Wilkendorf, J. Lorenzana, M. Aïn, G.J. McIntyre, M. Behruzi, G. Heger, G. Dhalenne, and A. Revcolevschi, Phys. Rev. B **54**, 1105 (1996).

[35] A.C. Komarek, T. Taetz, M.T. Fernández-Díaz, D.M. Trots, A. Möller, and M. Braden. Phys. Rev. B **79**, 104425 (2009).

[36] T. Yildirim. Phys. Rev. Lett. **1**01, 057010, (2008).